Combustion and Flame 262 (2024) 113372

Contents lists available at ScienceDirect

Combustion and Flame

journal homepage: www.sciencedirect.com/journal/combustion-and-flame

Combustion behavior of aluminized metal iodate composites. Part 1: Decomposition mechanism of metal iodates

Yujie Wang, Keren Shi, George Issac Paul, Prithwish Biswas, Michael R. Zachariah *

University of California, Riverside, CA 92521, United States

ARTICLE INFO

Keywords:
Metal iodate
Decomposition
Mechanism
Iodine release
Thermodynamic prediction

ABSTRACT

Metal iodates are candidates of high temperature biocidal oxidizing agents owing to their high iodine and oxygen content. Here we explore the high temperature decomposition mechanism of alkali and alkaline metal iodates ($LiIO_3$, $NaIO_3$, KIO_3, $Mg(IO_3)_2$, and $Ca(IO_3)_2$). Temperature-jump/time-of-flight mass spectrometry (T-Jump/TOFMS) measurements reveal that while all of these iodates release O_2, only $Mg(IO_3)_2$, $Ca(IO_3)_2$, and $LiIO_3$ release significant amount of I_2 and there is minimal I_2 release from $NaIO_3$ and KIO_3. Thermogravimetric-differential scanning calorimetry (TGA-DSC) measurement and X-ray diffraction (XRD) analysis of temperature dependent condensed phase species demonstrates the presence of two different decomposition pathways of metal iodates. $LiIO_3$, $Mg(IO_3)_2$, and $Ca(IO_3)_2$, follow a two-step decomposition pathway: (1) Decomposition from metal iodate (MIO_3, *M*=Mg, Ca, and Li) into metal orthoperiodate ($M_x(IO_6)_y$) accompanied by I_2 and O_2 release, and (2) decomposition from metal orthoperiodate to metal oxide (MO) accompanied by I_2 and O_2 release. $NaIO_3$ and KIO_3 follow a one-step decomposition pathway, where they decompose into NaI and KI, respectively, simultaneously releasing O_2. Decomposition temperatures are estimated from thermodynamic data and compared between different decomposition pathways to predict which pathway is more favorable during decomposition. These estimations predict the decomposition pathway of the investigated metal iodates as they are largely consistent with the experimental results. This study unveils a simple strategy for predicting whether a metal iodate is a promising biocidal agent by assessing its feasibility of I_2 release.

1. Introduction

Biological weapons pose a significant challenge to the global security. Therefore, it is essential to develop a strategy to deactivate or neutralize these highly dangerous bioagents. Halogen-containing fungicides, such as HF and chlorine-containing species, are effective in destroying bacteria [1,2]. However, their application is limited by potential toxicity and causticity. Iodine, while not benign to the environment has at least a significantly diminished footprint while still effective as a biocide. Iodine can react with cellular nucleic acids and thiol groups in enzymes and proteins after penetrating the cell wall of microorganisms, which leads to the structure disorder of microorganisms that eventually results in their inactivation [2]. Iodine has been proven to be an extremely effective biocidal agent as a very low concentration of I_2 (<15 ppm) with a high neutralization of 99.999 % for certain bacteria and viruses in 10 min at 25 °C [3]. However, application of molecular iodine as a biocidal agent is inconvenient as it sublimes at room temperature due to its high vapor pressure. Also, these conventional disinfectants with halogen-containing fungicides are often inefficient as they are difficult to be implemented for large-scale microorganism deactivation over a short time.

An alternative strategy for deactivating microorganism is the application of thermal energy over a short period of time, most conventionally though energetic materials [4]. Nevertheless, this strategy is likely insufficient for complete neutralization due to the transient nature of the thermal event, and the possibility of not homogeneously delivering the thermal pulse over the whole target region [4,5]. Based on the advantages and disadvantages of these two strategies, the development of agent defeat weapons (ADWs) that remain active for an extended period of time post-thermal pulse, has been proposed [3,6]. Therefore, consideration has been given to energetic systems with high energy density and iodine content, and various systems have been explored. Energetic composites containing I_2 have been prepared by mechanical milling and their combustion and biocidal effectiveness investigated [7–11]. However, these composites are unstable over long time storage and an additional oxidizer is required for the combustion to occur. I_2O_5

* Corresponding author.
E-mail address: mrz@engr.ucr.edu (M.R. Zachariah).

https://doi.org/10.1016/j.combustflame.2024.113372
Received 31 December 2023; Received in revised form 8 February 2024; Accepted 11 February 2024
Available online 15 February 2024

has received considerable attention due to its high iodine content and strong oxidizing property [12]. Clark et al. combined Al with I_2O_5 and investigated the destruction of spore forming bacteria [13]. Our group tuned the reactivity and energy release rate of energetic composites containing I_2O_5 by varying the fuel composition [14]. Nevertheless, the hygroscopic nature of I_2O_5 largely limits its practical application. Ideally, one desires a material which undergoes a highly exothermic redox reaction, contains a high content of iodine, releases molecular iodine, easy to handle, and can be stored over a long period.

Recently, metal iodates have attracted attention for this purpose due to their strong oxidizing property and high iodine content [4,5,15]. Combustion characteristics and iodine release investigations of energetic materials containing various metal iodates, such as $Bi(IO_3)_2$, $Ca(IO_3)_2$, $Fe(IO_3)_2$, $Cu(IO_3)_2$, and $AgIO_3$, have demonstrated that metal iodates are promising candidates in the application of ADWs [4,5,15–17]. Most noteworthy is that these studies show that not all of these iodates produce I_2 as the main iodine-containing species. Rather iodine can get kinetically trapped via formation of metal iodide [17]. However, a systematic investigation about the decomposition mechanism of metal iodates and the fundamental factors responsible for the decomposition pathway is lacking.

In this paper, we systematically investigate the decomposition mechanism of alkali and alkaline metal iodates ($LiIO_3$, $NaIO_3$, KIO_3, $Mg(IO_3)_2$, and $Ca(IO_3)_2$), which have high iodine and oxygen content (Fig. 1). Temperature-jump time of flight mass spectrometry (T-Jump/TOFMS) under rapid heating ($\sim 10^5$ K/s) conditions is utilized to analyze decomposition of metal iodates at high heating rate. Thermogravimetry-differential scanning calorimetry (TGA-DSC) is used to investigate the decomposition of metal iodates under slow heating (10 K/min) conditions to support the observation from T-Jump measurements. X-ray diffraction (XRD) is utilized to characterize the condensed phase species produced at different temperatures of interest with respect to TGA-DSC measurements. Thermodynamic prediction of iodate decomposition pathways is proposed.

2. Materials and methods

2.1. Materials

$NaIO_3$ (99 %) was purchased from Alfa Aesar. $LiIO_3$ (97 %), KIO_3 (≥98 %), $Ca(NO_3)_2{\cdot}4H_2O$ (≥99 %), $MgCl_2$ (≥98 %), NaI (≥99 %), and HIO_3 (≥99.5 %) were obtained from Sigma Aldrich. Ethanol (200 proof) was purchased from Koptec. NaOH (≥97 %), hexanes (99.9 %) and HPLC grade water were obtained from Fisher Scientific.

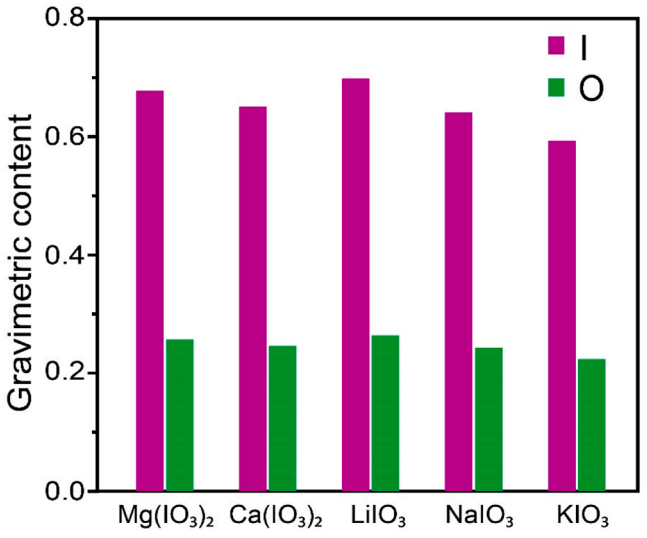

Fig. 1. Gravimetric iodine and oxygen content in alkali and alkaline metal iodates.

2.2. Size reduction of alkali metal iodates

Size reduction of $LiIO_3$, $NaIO_3$, and KIO_3 was performed via an aerosol spray pyrolysis (ASP) approach and was used for temperature jump time of flight mass spectrometry (T-Jump/TOFMS) [18–20]. Generally, 1 g of the as-received iodates were dissolved into 100 mL water and the resultant solution was sprayed into small droplets with an atomizer operating at ~35 psi using compressed air. The droplets passed through a silica-gel diffusion drier for removing water of the droplets, and then passed through a tube furnace (Lindberg/Blue) operating at 150 °C. The final product was collected on a filter paper. Sub-micron sized particles were obtained [20].

2.3. Synthesis of $Mg(IO_3)_2$ particles

50 mmol $MgCl_2$ was dissolved in 100 mL water and 100 mmol of NaOH was dissolved in 100 mL water. Then the NaOH solution was added to the $MgCl_2$ solution slowly. The obtained suspension was centrifuged at 7000 rpm for 5 min, the supernatant was discarded, and the precipitate was washed three times with 120 mL water each time. Then the precipitate was dried in oven operating at ~ 100 °C. The dried powder was weighed (28.6 mmol) and added to 200 mL water, the resultant cloudy suspension was stirred at ~350 rpm. Separately, HIO_3 (57.2 mmol) was dissolved in 50 mL water. Then the HIO_3 solution was added to the suspension slowly. At the end of HIO_3 solution, the suspension become transparent. The obtained $Mg(IO_3)_2$ solution was filtered before further utilization. $Mg(IO_3)_2$ particles were obtained via ASP with the furnace operating at 300 °C and then dried at 300 °C for 10 min in air. X-ray diffraction crystallography (XRD) confirms the final product is $Mg(IO_3)_2$ (Figure S1).

2.4. Synthesis of $Ca(IO_3)_2$ particles

Details of the preparation of $Ca(IO_3)_2$ particles can be found in ref. [21]. Briefly, 1 mmol of $Ca(NO_3)_2{\cdot}4H_2O$, 2 mmol of KIO_3, 0.5 mL ethanol, and three steel balls (7/32″ in diameter, purchased from GlenMills) were loaded into a plastic centrifuge tube (FisherBrand 2 mL), which was then milled with a Retsch CryoMill operated at ambient conditions for 20 min at a frequency of 25.0 Hz (25/s). The obtained slurry was centrifuged at 7000 rpm for 5 min and the resultant supernatant was discarded. The precipitate was washed three times with 30 mL water each time and the obtained sample was then dried overnight in a vacuum oven to remove free water and then baked in a tube furnace at 350 °C for 40 min in air to remove crystal water [16].

2.5. Characterization

Particle sizes were characterized by Scanning Electron Microscopy (SEM, NNS450) operating at 20 kV accelerating voltage. Temperature resolved analysis of as-received alkali metal iodates and synthesized alkaline metal iodates was conducted with a Netzsch STA 449 F3 Jupiter thermogravimetric analysis-differential scanning calorimetry (TGA-DSC) operating in argon with a flow rate of 50 mL/min at a heating rate of 10 K/min. It is noteworthy that the as-received samples of $LiIO_3$, $NaIO_3$, and KIO_3 are used for TGA-DSC, while for $Mg(IO_3)_2$ and $Ca(IO_3)_2$, the synthesized particles are used. Temperatures of interest for iterative analysis of each iodate were pinpointed from TGA-DSC profiles. Iodates were then heated in a tube furnace at these temperatures for 10 min ($LiIO_3$ at 650 °C, $NaIO_3$ at 575 °C, KIO_3 at 585 °C, $Mg(IO_3)_2$ at 650 °C, and $Ca(IO_3)_2$ at 640 °C) or 30 min ($LiIO_3$ at 900 °C, $Mg(IO_3)_2$ and $Ca(IO_3)_2$ at 800 °C) in argon and collected for X-ray diffraction crystallography (XRD PANanalytical Empyrean Series 2 diffractometer) analysis.

2.6. Temperature jump time of flight mass spectrometry (T-Jump/TOFMS)

The details of T-Jump/TOFMS can be found in previous publications from our group [22–24]. Briefly, size-reduced alkali metal iodate or synthesized alkaline metal iodate was suspended in hexane and sonicated briefly. The resultant suspension was coated to be a thin layer on a Pt wire (diameter=76 μm, 0.9–1.1 cm in length, OMEGA Engineering Inc.) that was soldered between two copper leads of a T-Jump probe. The probe was then loaded into the high-vacuum T-Jump MS chamber and the Pt wire was resistively heated with a 3 ms pulsed square wave signal from a direct current voltage supply. Thermometry of the Pt wire was acquired and temperature profile of the wire was obtained by applying the calibration relationship between the temperature of the wire and its corresponding resistance from the Callendar-Van Dusen equation. The temperature of the thin sample layer on Pt wire was roughly the same with the wire. A 70 eV electron gun ionizer was used to ionize gas phase species produced from heating. A Teledyne LeCroy 600 MHz oscilloscope was used for mass spectra collection as well as current and voltage readings over a 10 ms period with 0.1 ms interval.

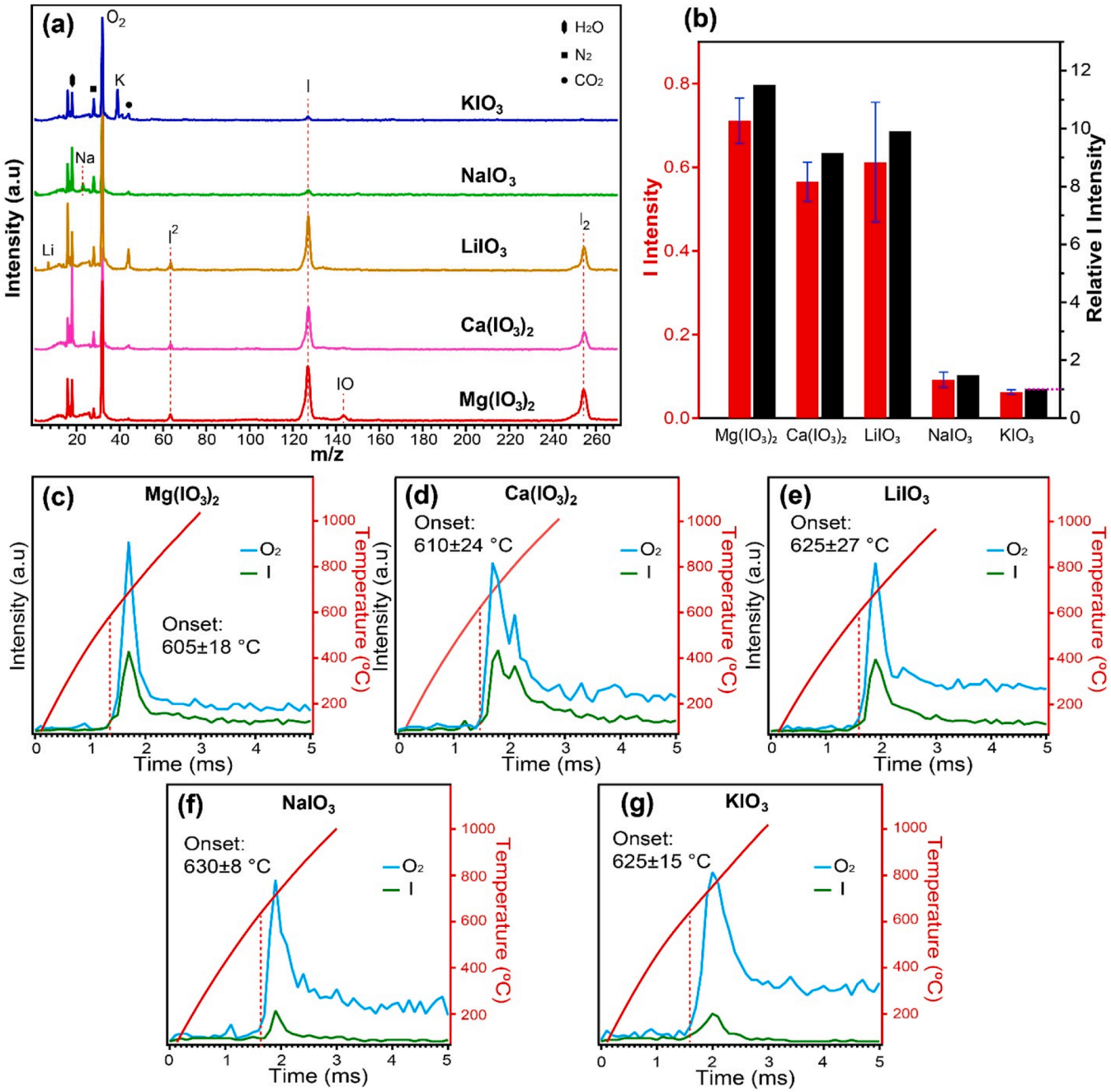

Fig. 2. Mass spectrum of rapidly heated alkali and alkaline metal iodates (a). Most notable mass species are labeled. The measured I release of these iodates and their relative intensity to KIO_3 (b). O_2 and I release over time and the corresponding heating profile of $Mg(IO_3)_2$ (c), $Ca(IO_3)_2$ (d), $LiIO_3$ (e), $NaIO_3$ (f), and KIO_3 (g). The onset release temperature averaged over a minimum of three experiments is labeled.

3. Result and discussion

3.1. Time-of-flight mass spectrometry under rapid heating rate (~10^5 K/s)

T-Jump/TOFMS was utilized to analyze the decomposition products of metal iodates under high heating rates (~10^5 K/s) and the resulting mass spectra are displayed in Fig. 2(a). O_2, as the main volatile species, appears in relatively large quantities for all the iodates. While for I, a representative of the I-containing species including I, and I_2, the peak intensities from $Mg(IO_3)_2$, $Ca(IO_3)_2$, and $LiIO_3$ are significantly higher than $NaIO_3$ and KIO_3. It is noteworthy that the formation of I arises from the ionization of I_2 by the electron gun ionizer. Semiquantitative analysis of the I release is conducted by measuring its peak intensity as well as relative intensity compared to KIO_3, as shown in Fig. 2(b), which clearly illuminates that the I release of $Mg(IO_3)_2$, $Ca(IO_3)_2$, and $LiIO_3$ is about 10 times higher than $NaIO_3$ and KIO_3. This analysis suggests the existence of two different decomposition mechanisms among these iodates. Stern reported that metal iodates may decompose according to three different routes: (a) metal iodide and O_2 are produced, (b) metal oxide, I_2, and O_2 are produced, and (c) metal orthoperiodate, I_2, and O_2 are produced [25]. Ito *et al.* and Morton et al. argued that orthoperiodate is not the final decomposition product, which can further decompose into metal oxide, I_2, and O_2 [26,27]. Therefore, based on the T-Jump/TOFMS analysis, it is proposed that $Mg(IO_3)_2$, $Ca(IO_3)_2$, and $LiIO_3$ follow pathway α, while $NaIO_3$ and KIO_3 follow pathway β.

$$\{Mg(IO_3)_2,\ Ca(IO_3)_2,\ \text{and } LiIO_3\} \qquad MIO_3 \rightarrow MO + O_2 + I_2 \qquad (\alpha)$$

$$\{NaIO_3 \text{ and } KIO_3\} \qquad MIO_3 \rightarrow MI + O_2 \qquad (\beta)$$

Where M=metal. It is also noteworthy that metal ions are present for alkali metal iodates (Li, Na, and K for $LiIO_3$, $NaIO_3$, and KIO_3, respectively), while for alkaline metal iodates, the peaks of their metal ions are absent. These metal signatures indicate the formation of metal iodides because the iodides are more volatile than oxides, which is due to the lower melting and boiling points of alkali metal iodides compared to their corresponding oxides, as evident in Table S1. O_2 and I release profiles of $Mg(IO_3)_2$, $Ca(IO_3)_2$, and $LiIO_3$ are displayed in Fig. 2(c)-(e) and these temporal profiles suggest that O_2 and I are released at the same temperature for all the three iodates, which will be discussed further in the subsequent sections. O_2 and I release profiles of $NaIO_3$ and KIO_3 displayed in Fig. 2(f) and (g) demonstrate the low intensity of I release over time.

3.2. Thermochemical analysis under slow heating rate (10 K/min)

Thermochemical analysis of the metal iodates is performed by slow heating TGA/DSC in an argon environment for supplementing the lack of gravimetric and calorimetric diagnostics from T-Jump/TOFMS. XRD is utilized to analyze the condensed phase products around featured temperature points of decomposition identified by TGA/DSC. TGA/DSC result and temperature dependent XRD analysis of $Mg(IO_3)_2$ are displayed in Fig. 3.

A two-step decomposition of $Mg(IO_3)_2$ is proposed by Ito *et al.*, where magnesium orthoperiodate ($Mg_5(IO_6)_2$) is produced from the first step while MgO is formed after the second step, and I_2 and O_2 are released at each step, as shown in Eq. (1) and (2) [26]. However, the verification of the decomposition products of each step is lacking.

$$Mg(IO_3)_2 = 0.2\ Mg_5(IO_6)_2 + 0.8\ I_2 + 1.8\ O_2 \qquad (1)$$

$$0.2\ Mg_5(IO_6)_2 = MgO + 0.2\ I_2 + 0.7\ O_2 \qquad (2)$$

The DSC in Fig. 3(a) reveals that $Mg(IO_3)_2$ does indeed follow a two-step decomposition process, although this two-step is not as evident in TGA. The measured mass losses of 71.9 % and 89.6 % after the first and the second step decomposition, respectively, are very close to the theoretical mass loss of $Mg(IO_3)_2$ at 69.7 % and 89.3 % predicated from Eq. (1) and (2), respectively. Also, as mentioned in 3.1, I_2 and O_2 are released at the same temperature for $Mg(IO_3)_2$ from T-Jump TOFMS (Fig. 2(c)), consistent with the proposed mechanism. XRD analysis of the solid-state products collected after each step in Fig. 3(b) illuminates that $Mg_5(IO_6)_2$ is formed at the end of the first decomposition step (650 °C), although MgO is also detected, indicating a portion of $Mg_5(IO_6)_2$ is further decomposed. After the second step (680 °C), MgO is produced. This analysis verifies the decomposition of $Mg(IO_3)_2$ follows Eq. (1) and (2), and the overall decomposition is consistent with the decomposition route (pathway (α)) proposed in 3.1.

Fig. 4(a) displays the TGA/DSC for the decomposition of $Ca(IO_3)_2$ as well as the XRD analysis of the solid product collected by the end of each mass loss step. Similar to $Mg(IO_3)_2$, $Ca(IO_3)_2$ demonstrates the previously documented two-step decomposition [27], and these two steps are shown in Eq. (3) and (4).

$$Ca(IO_3)_2 = 0.2\ Ca_5(IO_6)_2 + 0.8\ I_2 + 1.8\ O_2 \qquad (3)$$

$$0.2\ Ca_5(IO_6)_2 = CaO + 0.2\ I_2 + 0.7\ O_2 \qquad (4)$$

The measured mass loss of 64.5 % after the first decomposition step is close to the theoretically predicted mass loss of 66.9 %, and the measured mass loss of 85.4 % after the second decomposition step is nearly identical to the theoretically predicted mass loss of 85.6 %. XRD analysis reveals that $Ca_5(IO_6)_2$ is produced after the first decomposition step (640 °C) while the final product is CaO (740 °C). These results, combined with the observation that I_2 and O_2 are released at the same temperature from T-Jump TOFMS (Fig. 2(d)), confirm that the

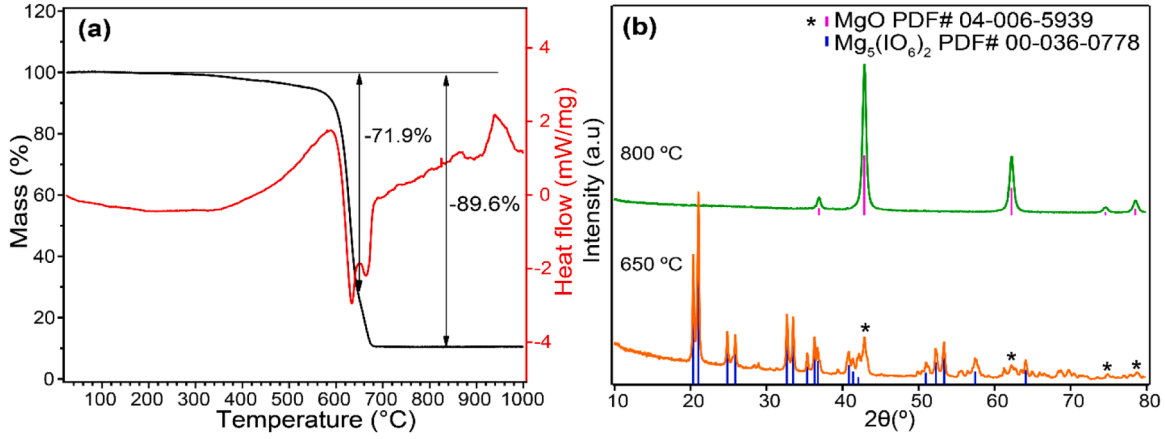

Fig. 3. TGA/DSC of $Mg(IO_3)_2$ under and argon environment (a), and temperature dependent XRD analysis of $Mg(IO_3)_2$ heated products (b).

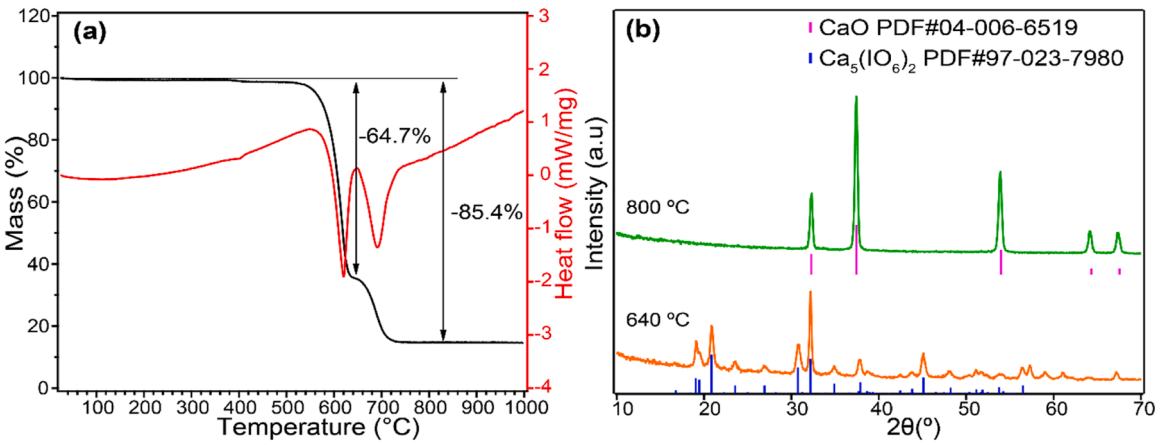

Fig. 4. TGA/DSC of $Ca(IO_3)_2$ under and argon environment (a), and temperature dependent XRD analysis of $Ca(IO_3)_2$ heated products (b).

decomposition of $Ca(IO_3)_2$ is consistent with the two-step decomposition mechanism.

As discussed in 3.1, $LiIO_3$, $Mg(IO_3)_2$, and $Ca(IO_3)_2$ demonstrate a similar decomposition characteristic from the T-Jump TOFMS analysis (Fig. 2), therefore it is proposed that the decomposition of $LiIO_3$ follows the two steps represented in Eq. (5) and (6) based on the decomposition process of $Mg(IO_3)_2$ and $Ca(IO_3)_2$.

$$LiIO_3 = 0.2\ Li_5IO_6 + 0.4\ I_2 + 0.9\ O_2 \quad (5)$$

$$0.2\ Li_5IO_6 = 0.5\ Li_2O + 0.1\ I_2 + 0.35\ O_2 \quad (6)$$

Fig. 5 displays the TGA/DSC of $LiIO_3$ as well as XRD analysis of temperature dependent decomposition products of $LiIO_3$. TGA/DSC of $LiIO_3$, as displayed in Fig. 5(a), shows a two-step mass loss process. The measured mass loss at the end of each step is 70.8 % and 92.5 %, respectively, which are approximate to the predicted theoretical mass loss of 71.7 % and 91.8 % according to Eq. (5) and (6), respectively. XRD analysis reveals that the solid product collected after the first decomposition (650 °C) is Li_5IO_6, consistent with the expectation from Eq. (5). The product from the second step that ends at 870 °C is a mixture of Li_2O, LiI, and undecomposed Li_5IO_6. While Li_2O and undecomposed Li_5IO_6 are expected to form based on Eq. (6), the presence of LiI suggests a different decomposition pathway from $Mg(IO_3)_2$ and $Ca(IO_3)_2$, whose final decomposition product does not contain MgI_2 and CaI_2, respectively. This difference will be discussed in more details in the subsequent section.

It has been demonstrated from T-Jump TOFMS, TGS/DSC, and XRD analysis that the decomposition of $LiIO_3$, $Mg(IO_3)_2$, and $Ca(IO_3)_2$ occur via two steps, with the first step forming metal orthoperiodate, I_2 and O_2, and the second step producing metal oxide, I_2 and O_2. $NaIO_3$ and KIO_3 are expected to follow a different decomposition pathway as they produce minimal I_2 during decomposition from the T-Jump TOFMS analysis (Fig. 2). TGA/DSC of $NaIO_3$, as displayed in Fig. 6, shows multiple-stepped mass loss. XRD analysis shows that the solid residue collected at the end of the first mass loss step (575 °C) is NaI. The attempt to collect residue at 900 °C was unsuccessful. The formation of NaI and the absence of intense I_2 peak from T-Jump TOFMS (Fig. 2) suggest the following decomposition of $NaIO_3$:

$$NaIO_3 = NaI + 1.5\ O_2 \quad (7)$$

Additionally, we observe Na peak from T-Jump/TOFMS (Fig. 2), which also indicates NaI formation. The theoretical mass loss based on Eq. (7) is 24.4 %, which is much lower than the measured first step mass loss of 53.7 %, and this is attributed to the sublimation of NaI [28,29]. The mass loss after the first step is attributed to the evaporation of NaI, whose TGA/DSC shows rapid mass loss after the melting point at 661.6 °C (Figure S2).

KIO_3 displays a similar decomposition mechanism to $NaIO_3$ based on the presence of metal ion peak and minimal release of iodine, as shown in Fig. 2. Therefore we expect the following decomposition pathway for KIO_3:

$$KIO_3 = KI + 1.5\ O_2 \quad (8)$$

TGA/DSC of KIO_3 displays a two-stepped mass loss (Fig. 7(a)). The measured mass loss of the first step that ends at 585 °C is 22.4 %, which

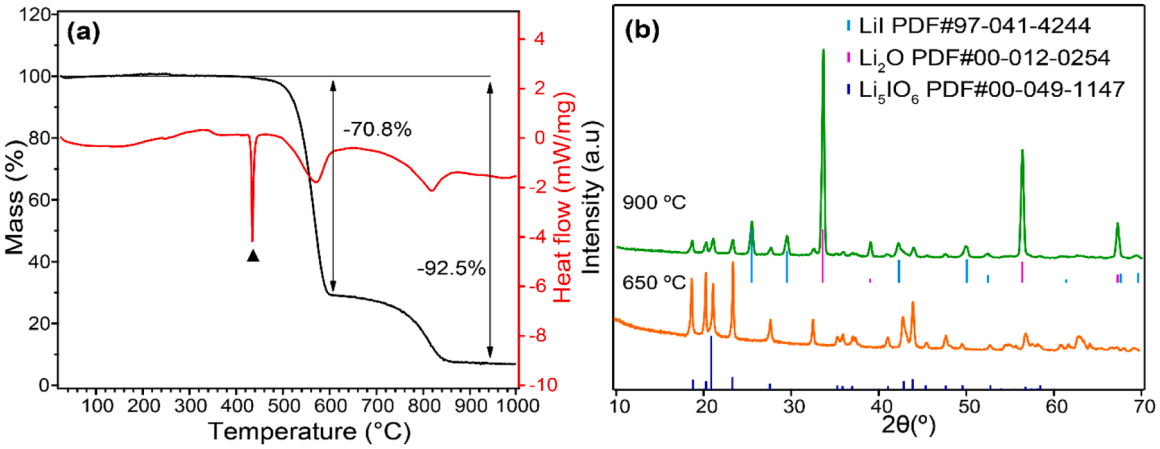

Fig. 5. TGA/DSC of $LiIO_3$ under and argon environment (a), and temperature dependent XRD analysis of $LiIO_3$ heated products (b). ▲indicates melting of $LiIO_3$ [20]..

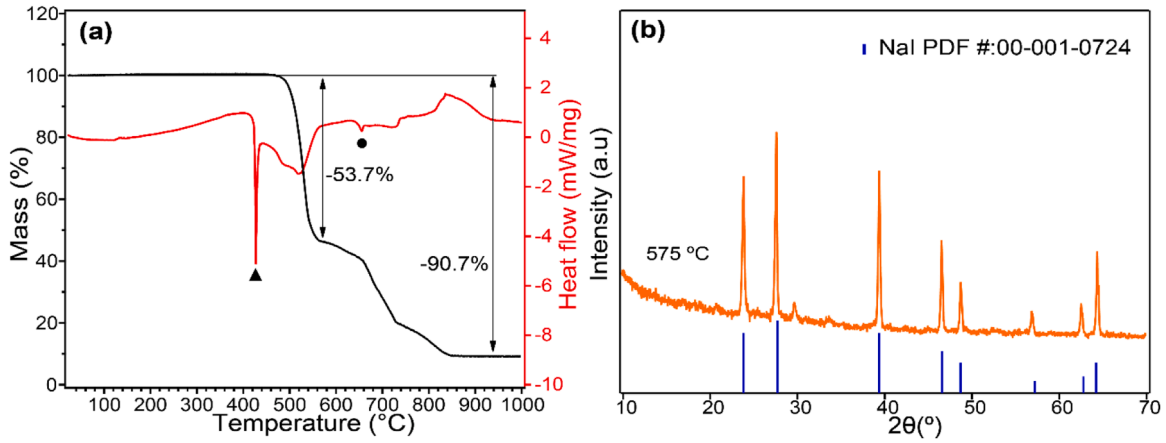

Fig. 6. TGA/DSC of $NaIO_3$ under and argon environment (a), and temperature dependent XRD analysis of $NaIO_3$ heated products (b). ▲indicates melting of $NaIO_3$ and ● indicates melting of produced NaI [20,30]..

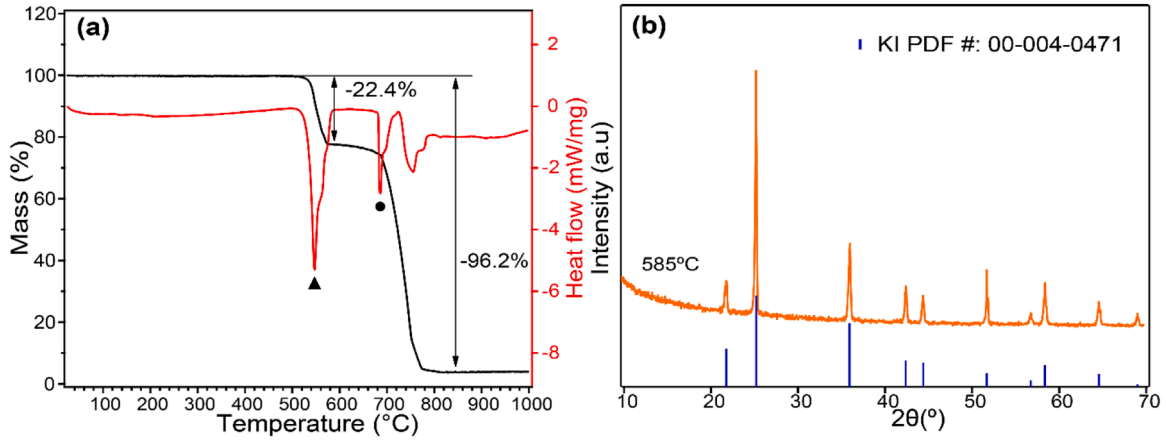

Fig. 7. TGA/DSC of KIO_3 under and argon environment (a), and temperature dependent XRD analysis of KIO_3 heated products (b). ▲indicates melting of KIO_3 and ● indicates melting of produced KI [20,30]..

is the same with the theoretical mass loss of 22.4 % predicted from Eq. (8). XRD analysis (Fig. 7(b)) of decomposition product after the first mass loss step reveals the formation of KI. The second mass loss step in TGA/DSC is attributed to the evaporation of KI [30].

3.3. *Thermodynamic prediction of iodate decomposition mechanism*

Gibbs free energy change determines whether a reaction is feasible. A negative Gibbs free energy indicates a spontaneous reaction [31]. Decomposition of metal iodates can follow pathway α, which produces metal oxide, O_2, and I_2, or β, which leads to metal iodide and O_2. For simplicity, all the calculations for Gibbs free energy change is performed with standard values of ΔH and ΔS at room temperature. All the calculated values of ΔG are positive as none of the iodates decompose at room temperature, as shown in Figure S3. The decomposition temperatures of both pathways are estimated, assuming ΔG is 0, while ΔH and ΔS are held constant. These estimated decomposition temperatures are then normalized to the measured decomposition temperatures from T-Jump MS and are displayed in Fig. 8. For $Mg(IO_3)_2$ and $Ca(IO_3)_2$, the estimated decomposition temperature of pathway α is lower than pathway β, suggesting that pathway α is more favorable. This finding is consistent with the observations from T-Jump TOFMS, TGA/DSC and XRD. In the case of $NaIO_3$ and KIO_3, pathway β is the more favorable due to its significantly lower estimated decomposition temperature than pathway α, which is also supported by evidence from T-Jump TOFMS, TGA/DSC and XRD. However, for $LiIO_3$, the estimated decomposition

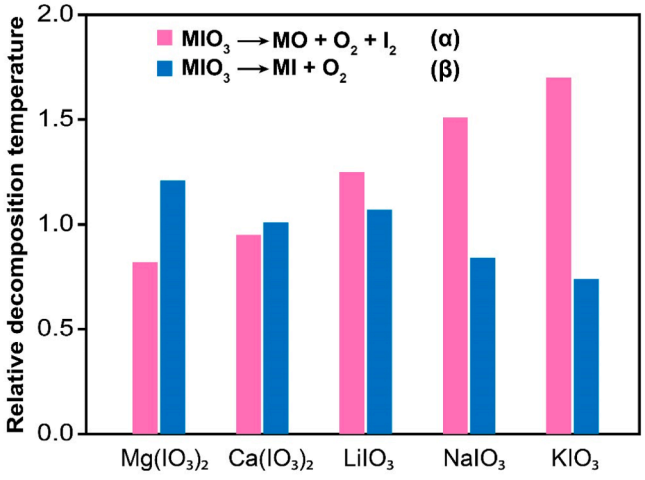

Fig. 8. Calculated decomposition temperature of metal iodates assuming Gibbs free energy change being zero at room temperature relative to the measured decomposition temperature from T-Jump MS for different decomposition pathways. More details about the calculation can be found in Table S2.

temperature of pathway α is higher than pathway β, indicating that pathway β is more favorable. This contradicts the experimental result demonstrating that pathway α is more feasible. This discrepancy is not well understood. Overall, the trend is clear that as the metal descends within the same group, from Mg to Ca and Li to K, the estimated decomposition temperature of pathway α increases, while the calculated decomposition temperature of pathway β decreases. Consequently, pathway α becomes less favorable while pathway β becomes more favorable as metal moves downward in the same group. A similar argument can be made that when metal moves rightward in the same period, from Na to Mg and K to Ca, pathway β becomes less favorable while pathway α becomes more favorable.

4. Conclusions

This study investigates the decomposition mechanism of alkali and alkaline metal iodates ($LiIO_3$, $NaIO_3$, KIO_3, $Mg(IO_3)_2$, and $Ca(IO_3)_2$). T-Jump TOFMS demonstrates that all iodates release O, but not all iodates release I_2. $Mg(IO_3)_2$, $Ca(IO_3)_2$, and $LiIO_3$ release significant amount of I_2, while $NaIO_3$ and KIO_3 have minimal I_2 release. TGA/DSC measurement of metal iodates and XRD analysis of the temperature dependent condensed phase species reveals that the decomposition of these metal iodates follows different pathways. $Mg(IO_3)_2$, $Ca(IO_3)_2$, and $LiIO_3$ follow a two-step decomposition pathway: (1) Decomposition from metal iodates (MIO_3. *M*=Mg, Ca, and Li) into metal orthoperiodate ($M_x(IO_6)_y$) with I_2 and O_2 release, and (2) decomposition from metal orthoperiodate to metal oxide (MO) with I_2 and O_2 release. $NaIO_3$ and KIO_3 follow a one-step decomposition pathway, where they decompose into NaI and KI, respectively, with O_2 release. Thermodynamic predictions of decomposition pathways are made by comparing decomposition temperatures estimated from thermodynamic data, and these estimations roughly predict the decomposition pathway of the investigated metal iodates. This study reveals that not all metal iodates are potential candidates for biocidal application and provides a simple strategy to predict the feasibility of I_2 release from metal iodates.

Novelty and significance statement

Iodine has been proven to be an effective biocidal agent. However, direct application of molecular iodine is inconvenient due to its sublimation at room temperature and often inefficient for large-scale microorganism deactivation. One strategy to address these issues is to develop an energetic composite that releases iodine along with a thermal pulse. Previous studies have shown that certain metal iodates exhibit potential suitability for this application, although it is noteworthy that not all metal iodates share this characteristic. Unfortunately, a systematic study regarding the decomposition mechanism of metal iodates is lacking. The present study provides experimental data to prove that metal iodates follow two different decomposition pathways. Additionally, a simple thermodynamic calculation is proposed to predict which decomposition pathway is more favorable for metal iodates.

Author contributions statement

Y.W designed and performed experiment, analyzed data and wrote the paper. K.S performed characterization and reviewed the paper. G.P performed experiment and reviewed the paper. P.B performed characterization and reviewed the paper. M.R.Z investigated and supervised the research, reviewed and edited the paper.

Declaration of competing interest

On behalf of all the authors, we declare no conflict of interest. This work is original and has not been considered for publication elsewhere.

Acknowledgement

This work was supported by the DTRA-URA: Center for Materials Science Under Extreme Environments.

Supplementary materials

Supplementary material associated with this article can be found, in the online version, at doi:10.1016/j.combustflame.2024.113372.

References

[1] M.J. Gray, W.-Y. Wholey, U. Jakob, Bacterial responses to reactive chlorine species, Annu. Rev. Microbiol. 67 (2013) 141–160.
[2] J. Chang, G. Zhao, X. Zhao, C. He, S. Pang, J.M. Shreeve, New promises from an old friend: iodine-rich compounds as prospective energetic biocidal agents, Acc. Chem. Res. 54 (2021) 332–343.
[3] T. Kaiho, Iodine Chemistry and Applications, John Wiley & Sons, 2014.
[4] X. Hu, J.B. DeLisio, X. Li, W. Zhou, M.R. Zachariah, Direct deposit of highly reactive Bi(IO3)3- polyvinylidene fluoride biocidal energetic composite and its reactive properties, Adv. Eng. Mater. 19 (2017) 1500532.
[5] H. Wang, G. Jian, W. Zhou, J.B. DeLisio, V.T. Lee, M.R. Zachariah, Metal iodate-based energetic composites and their combustion and biocidal performance, ACS Appl. Mater. Interfaces 7 (2015) 17363–17370.
[6] M. Wheelis, Deadly Cultures: Biological Weapons Since 1945, Harvard University Press, 2006.
[7] Y. Aly, S. Zhang, M. Schoenitz, V.K. Hoffmann, E.L. Dreizin, M. Yermakov, R. Indugula, S.A. Grinshpun, Iodine-containing aluminum-based fuels for inactivation of bioaerosols, Combust. Flame 161 (2014) 303–310.
[8] S. Wang, A. Abraham, Z. Zhong, M. Schoenitz, E.L. Dreizin, Ignition and combustion of boron-based Al·B·I2 and Mg·B·I2 composites, Chem. Eng. J. 293 (2016) 112–117.
[9] S. Zhang, M. Schoenitz, E.L. Dreizin, Iodine release, oxidation, and ignition of mechanically alloyed Al—I composites, J. Phys. Chem. C 114 (2010) 19653–19659.
[10] S.A. Grinshpun, A. Adhikari, M. Yermakov, T. Reponen, E. Dreizin, M. Schoenitz, V. Hoffmann, S. Zhang, Inactivation of aerosolized Bacillus atrophaeus (BG) endospores and MS2 viruses by combustion of reactive materials, Environ. Sci. Technol. 46 (2012) 7334–7341.
[11] S. Zhang, C. Badiola, M. Schoenitz, E.L. Dreizin, Oxidation, ignition, and combustion of Al·I2 composite powders, Combust. Flame 159 (2012) 1980–1986.
[12] K.S. Martirosyan, L. Wang, D. Luss, Novel nanoenergetic system based on iodine pentoxide, Chem. Phys. Lett. 483 (2009) 107–110.
[13] B.R. Clark, M.L. Pantoya, The aluminium and iodine pentoxide reaction for the destruction of spore forming bacteria, Phys. Chem. Chem. Phys. 12 (2010) 12653–12657.
[14] F. Xu, P. Biswas, G. Nava, J. Schwan, D.J. Kline, M.C. Rehwoldt, L. Mangolini, M. R. Zachariah, Tuning the reactivity and energy release rate of I2O5 based ternary thermite systems, Combust. Flame 228 (2021) 210–217.
[15] C.E. Johnson, K.T. Higa, Iodine-rich biocidal reactive materials, MRS Online Proc. Libr. 1521 (2013) 307.
[16] H. Wang, D.J. Kline, M. Rehwoldt, M.R. Zachariah, Ignition and combustion characterization of Ca(IO3)2-based pyrotechnic composites with B, Al, and Ti, Propellants Explos. Pyrotech. 43 (2018) 977–985.
[17] K.T. Sullivan, N.W. Piekiel, S. Chowdhury, C. Wu, M.R. Zachariah, C.E. Johnson, Ignition and combustion characteristics of nanoscale Al/AgIO3: a potential energetic biocidal system, Combust. Sci. Technol. 183 (2010) 285–302.
[18] W. Zhou, J.B. DeLisio, X. Wang, M.R. Zachariah, Reaction mechanisms of potassium oxysalts based energetic composites, Combust. Flame 177 (2017) 1–9.
[19] T. Wu, A. SyBing, X. Wang, M.R. Zachariah, Aerosol synthesis of phase pure iodine/iodic biocide microparticles, J. Mater. Res. 32 (2017) 890–896.
[20] Y. Wang, H. Wang, F. Xu, P. Ghildiyal, M.R. Zachariah, Effect of alkali metal perchlorate and iodate type on boron ignition: the role of oxidizer phase change, Chem. Eng. J. 446 (2022) 136786.
[21] H. Wang, J.B. DeLisio, T. Wu, X. Wang, M.R. Zachariah, One-step solvent-free mechanochemical synthesis of metal iodate fine powders, Powder Technol. 324 (2018) 62–68.
[22] G. Jian, N.W. Piekiel, M.R. Zachariah, Time-resolved mass spectrometry of nano-Al and nano-Al/CuO thermite under rapid heating: a mechanistic study, J. Phys. Chem. C 116 (2012) 26881–26887.
[23] G. Jian, S. Chowdhury, K. Sullivan, M.R. Zachariah, Nanothermite reactions: is gas phase oxygen generation from the oxygen carrier an essential prerequisite to ignition? Combust. Flame 160 (2013) 432–437.
[24] M.C. Rehwoldt, Y. Wang, F. Xu, P. Ghildiyal, M.R. Zachariah, High-temperature interactions of metal oxides and a PVDF binder, ACS Appl. Mater. Interfaces (2022).
[25] K.H. Stern, High Temperature Properties and Thermal Decomposition of Inorganic Salts with Oxyanions, CRC Press, 2000.
[26] N. Ito, K. Obata, Y. Shindo, T. Hakuta, H. Yoshitome, Catalytic thermal decomposition of magnesium iodate in the presence of metal oxides or carbon, Thermochim. Acta 73 (1984) 33–40.
[27] R.C.B. Morton, V.E. McKelvey, United States Department of the Interior, (n.d.).

[28] K. Hilpert, Vaporization of sodium iodide and thermochemistry of (NaI)2(g) and (NaI)3(g): an experimental and theoretical study, Berichte Bunsenges. Für Phys. Chem. 88 (1984) 132–139.
[29] L.N. Kotter, L.J. Groven, Boron carbide based biocide compositions: a study of iodate particle size on combustion and iodine output, Propellants Explos. Pyrotech. 45 (2020) 509–516.
[30] W.M. Haynes, CRC Handbook of Chemistry and Physics, 95th Ed., CRC Press, Hoboken, 2014.
[31] J.M. Smith, H.C.V. Ness, M. Abbott, Introduction to Chemical Engineering Thermodynamics, McGraw-Hill Education, 2005.